

# Anderson localization effects on doped Hubbard model

Nathan Giovanni,<sup>1,2</sup> Marcello Civelli,<sup>2</sup> and Maria C. O. Aguiar<sup>1,2</sup>

<sup>1</sup>*Departamento de Física, Universidade Federal de Minas Gerais,  
C.P. 702, 30123-970, Belo Horizonte, MG, Brazil*

<sup>2</sup>*Université Paris-Saclay, CNRS, Laboratoire de Physique des Solides, 91405, Orsay, France*  
(Dated: August 25, 2020)

We derive the disorder vs. doping phase diagram of the doped Hubbard model via Dynamical Mean Field Theory combined with Typical Medium Theory, which allows the description of both Mott (correlation driven) and Anderson (disorder driven) metal-insulator transitions. We observe a metal-insulator transition to an Anderson-Mott insulator for increasing disorder strength at all interactions. In the weak correlation regime and rather small doping, the Anderson-Mott insulator displays properties which are alike to the ones found at half-filling. This is characterized by the presence of empty sites that give rise to a V-shaped electronic density of states. If we further increase either the doping or the correlation however, an Anderson-Mott phase of different kind arises for sharply weaker disorder strength. This phase occupies the largest part of the phase diagram in the strong correlation regime, and it has both Anderson and Mott character, but empty sites and the V-shaped density of states are absent.

## I. INTRODUCTION

Mott proposed that electronic correlations can drive a system through a metal-insulator transition (MIT).<sup>1</sup> Hubbard showed that in a half-filled lattice this transition happens when the local correlation contribution is larger than a critical value.<sup>2</sup> Large correlations are present when a material has a narrow valence band, in which case electrons spread less in the lattice and thus interact more between them, favoring the formation of a Mott insulator.<sup>3,4</sup> Transition metal oxides are examples of materials where this Mott physics plays a key-role.<sup>4-6</sup>

In the opposite limit i.e. non-interacting electrons, the presence of disorder can also drive the systems into an insulating phase - the Anderson insulator in this case.<sup>7,8</sup> Even though there have been improvements in sample growing techniques, effects of disorder are hardly avoidable. Therefore, in doped Mott systems too, disorder plays a non-trivial role, interplaying with doping and correlation. These effects are hard to analyze from both experimental and theoretical perspectives.

In experiments, correlation and disorder effects interplay, for example, in the MIT observed in doped semiconductors, such as Si:P and Si:B,<sup>9</sup> and in dilute two dimensional electron and hole systems, like silicon metal-oxide-semiconductor field-effect transistors (MOSFETs) and semiconductor heterostructures.<sup>10,11</sup> More recently, the observation of disorder induced insulator to metal transition has been reported in Mott systems, such as layered dichalcogenide 1T-TaS<sub>2</sub><sup>12</sup> and Ru-substituted Sr<sub>3</sub>Ir<sub>2</sub>O<sub>7</sub>.<sup>13</sup>

From the theoretical viewpoint, the interplay between correlation and disorder can be well described by the Hubbard model solved within extensions of Dynamical Mean Field Theory (DMFT).<sup>14</sup> DMFT description of disorder is equivalent to that of the coherent potential approximation (CPA)<sup>15</sup> and, as such, misses to describe Anderson localization effects.<sup>7</sup> To circumvent this problem, a mean field treatment of disorder, the so-

called Typical Medium Theory (TMT), has been proposed and proved capable of describing the disorder-induced localization.<sup>16-18</sup> The combination of TMT with DMFT has contributed to our understanding of the non-trivial interplay between correlation and disorder localization effects.<sup>19-23</sup>

In previous works based on DMFT-TMT, an insulating phase which is a mixture of Mott and Anderson insulators has been observed at half-filling.<sup>20,24</sup> This Anderson-Mott insulator (AMI) is characterized by the presence of singly-occupied sites, like in a Mott insulator, but has also doubly-occupied and empty sites, like in an Anderson insulator. Here, we extend these works by investigating the doped-dependent phase diagram of the disordered Hubbard model.

According to our main results, in the small correlated regime and moderately low doping, disorder induces an AMI which is similar to the one found in the disorder-driven Anderson-Mott transition at half-filling. This AMI displays a V-shaped density of states (DOS) around the Fermi energy. We shall show that this is a consequence of the appearance of empty sites, and it is therefore a disorder-induced Anderson effect. This V-shaped DOS is in agreement with previous quantum Monte Carlo (QMC) and exact-diagonalization calculations for the two-dimensional disordered Hubbard model.<sup>25</sup> In this reference, however, the disorder versus doping phase diagram was not fully explored. In this paper, we study the complete phase diagram as a function of interaction, disorder, and doping. As the number of carriers and/or the electronic correlation increases, the empty sites become occupied and the V-shaped DOS is no more observed. For strong correlations, we obtain then an AMI which is different from the one observed at half-filling or in the weak correlation regime. This phase sets in a large part of the disorder versus doping phase diagram at much weaker disorder strengths than the V-shaped DOS AMI. This shows in particular that the doped strongly correlated metal is more susceptible to Mott-Anderson

induced localization than the weakly correlated metal.

The paper is organized as follows. In the next section we define the model and describe the methodology used to solve it. Section III is devoted to the presentation and discussion of the disorder versus doping phase diagrams built for different values of the electronic correlation. In subsection III A, we study the V-shaped DOS region of the phase diagrams, that sets in at small doping and large disorder interaction and displays properties similar to the ones of the AMI known at half-filling. In Sec. IV we explore in details the results obtained in the strong correlation regime  $U/4t = 3$  and characterize the rising of a different disorder-driven AMI, which has no empty sites and thus no V-shaped DOS. Finally, Sec. V contains a summary of our conclusions.

## II. MODEL AND METHODOLOGY

We focus on the effects of doping the Anderson-Hubbard model (AHM), which is given by the Hamiltonian

$$H = -t \sum_{\langle ij \rangle \sigma} (c_{i\sigma}^\dagger c_{j\sigma} + c_{j\sigma}^\dagger c_{i\sigma}) + U \sum_i n_{i\uparrow} n_{i\downarrow} + \sum_{i\sigma} (\varepsilon_i - \mu) n_{i\sigma}, \quad (1)$$

where  $c_{i\sigma}^\dagger$  ( $c_{i\sigma}$ ) creates (destroys) an electron with spin  $\sigma$  on site  $i$ ,  $n_{i\sigma} = c_{i\sigma}^\dagger c_{i\sigma}$ ,  $t$  is the hopping amplitude for nearest neighbor sites,  $U$  is the on-site repulsion,  $\varepsilon_i$  is the random on-site energy, which follows a uniform distribution  $P(\varepsilon)$  centered in  $\varepsilon = 0$  and of width  $W$ .  $\mu$  is the chemical potential, which sets the doping according to  $\delta = 2 \langle n_{i\sigma} \rangle - 1$ , with respect to the parent compound ( $\delta = 0$ ) which is nominally at half-filling  $\langle n_{i\sigma} \rangle = 1/2$ . We fix here and through the paper the non-interacting bandwidth  $B = 4t$  as energy unit. Temperature is set to  $T = 0.01$ . We consider the paramagnetic solution of the model, observed experimentally, for example, in  $V_2O_3$  at high temperatures.<sup>26,27</sup>

To be able to describe the correlated Mott transition, we use DMFT<sup>14</sup>. In this methodology, a clean lattice problem is mapped onto an auxiliary single-impurity problem, whose conduction electron bath is determined self-consistently. In the disordered case, the mapping is onto an ensemble of impurity problems, each corresponding to a different value of the parameter that is randomly distributed [on-site energy  $\varepsilon_i$  in eq. (1)]. DMFT self-consistency involves taking an (arithmetic) average over this ensemble. However, average values do not describe well the asymmetric distributions generated by strong disorder.<sup>7</sup> As a drawback, DMFT is not able to capture the Anderson transition. By considering the most probable or typical value over the ensemble, instead of the average one, TMT treatment of disorder has been proved capable of describing Anderson localization.<sup>16,17</sup> Here we use the combination of DMFT and TMT to solve the

AHM (eq. 1) and describe the interplay between correlation and disorder induced localization.

Within DMFT-TMT, all the impurities of the ensemble “see” a typical effective medium, which is self-consistently calculated, as follows. We start by considering an initial function  $\Delta(\omega)$  that describes this effective medium. By solving the ensemble of single-impurity problems in the presence of this bath, we obtain the self-energies  $\Sigma_i(\omega)$  and the local Green’s functions

$$G(\omega, \varepsilon_i) = [\omega - \varepsilon_i - \Delta(\omega) - \Sigma_i(\omega)]^{-1}, \quad (2)$$

from which local spectra  $\rho(\omega, \varepsilon_i) = -\frac{1}{\pi} \text{Im} G(\omega, \varepsilon_i)$  are calculated. In each DMFT-TMT iteration, an effective medium is calculated: this is given by the *typical or most probable value* of local impurity spectrum, estimated by taking a *geometric average* over the different impurity problems. Precisely, the typical DOS is obtained by the geometric average of  $\rho(\omega, \varepsilon)$ ,

$$\rho_{typ}(\omega) = \exp \left[ \int d\varepsilon P(\varepsilon) \ln \rho(\omega, \varepsilon) \right]. \quad (3)$$

The typical Green’s function is then calculated through a Hilbert transform,

$$G_{typ}(\omega) = \int_{-\infty}^{\infty} d\omega' \frac{\rho_{typ}(\omega')}{\omega - \omega'}. \quad (4)$$

As reference case, we consider the Bethe lattice with infinite coordination number, which corresponds to a semi-circular DOS in the non-interacting limit.<sup>14</sup> In this particular case, we close the self-consistent loop by obtaining the new bath function as  $\Delta(\omega) = t^2 G_{typ}(\omega)$ .

The typical DOS  $\rho_{typ}(\omega)$  takes into account only extended states of the system. It is thus critical at the disorder-induced transition, as the system states become localized and  $\rho_{typ}(\omega)$  is then expected to go to zero. The (arithmetic) average DOS, which is for instance directly detected in spectroscopic experiments, can also be calculated from the DOS of the single-impurity problems, as follows:

$$\rho_{av}(\omega) = \int d\varepsilon P(\varepsilon) \rho(\omega, \varepsilon). \quad (5)$$

It considers both extended and localized states of the system<sup>20</sup> and remains finite at disordered induced MIT. This quantity however goes to zero around the Fermi level by increasing correlation. It signals therefore the correlated-driven Mott MIT.<sup>14</sup> In the next sections, we shall analyze both quantities  $\rho_{typ}(\omega)$  and  $\rho_{av}(\omega)$  to characterize the phases appearing in the AHM phase diagram.

Since the DMFT-TMT self-consistent condition is based on the DOS, it is advantageous to solve the single-impurity problems on the real axis, to avoid an analytic continuation procedure. Here, we solve these auxiliary problems by using perturbation theory in  $U$ .<sup>28,29</sup> Away from half-filling, the second order contribution in  $U$  is given by an expression that interpolates between

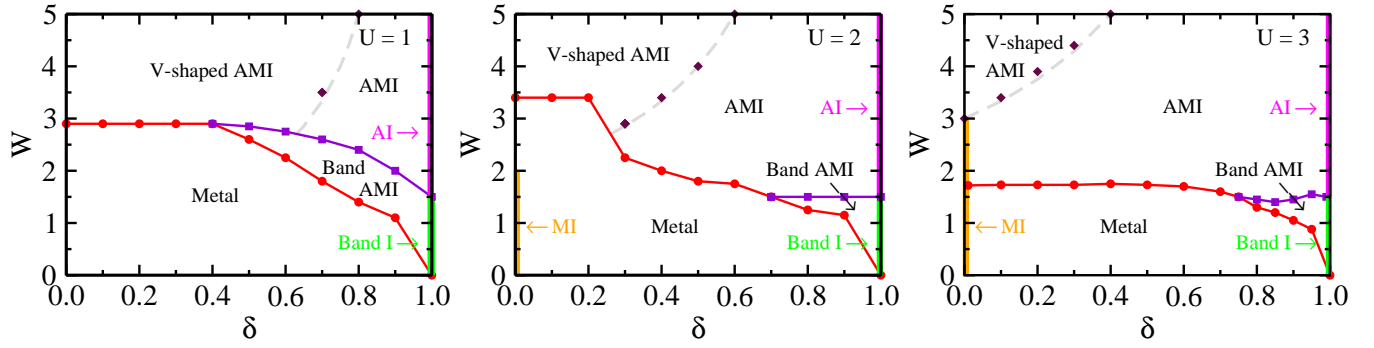


FIG. 1. Disorder ( $W$ ) versus doping ( $\delta$ ) phase diagram of the doped Anderson-Hubbard model obtained within DMFT-TMT for  $U = 1$ ,  $U = 2$ , and  $U = 3$  at  $T = 0.01$ . "A" stands for Anderson, "M" for Mott, and "I" for insulator. Inside the Anderson-Mott insulator phase, we have a region where the DOS around the Fermi level presents a V-shaped form; this region is identified as V-shaped AMI in the figure. Another region inside AMI is that of a band AMI. See text for a complete description of the different phases and regions.

the known results at high frequencies and at the atomic limit.<sup>28,29</sup> Comparisons of this approximation with exact diagonalization<sup>29</sup> and QMC<sup>30</sup> results give us confidence in it. Besides directly providing the spectra, this method has the advantage of being numerically fast to allow us to build the phase diagram of disordered problems. For each set of the model parameters, we typically solve hundreds of single-impurity problems in each DMFT-TMT iterative step. The single-impurity code used in this work was developed by Jaksa Vučičević and Darko Tanasković, from the Institute of Physics in Belgrade, Serbia, and was previously used by one of us in Ref. 22.

### III. DISORDER VS. DOPING PHASE DIAGRAMS

In Fig. 1, we present the disorder  $W$  vs. doping  $\delta$  phase diagram of the doped AHM obtained for three different values of correlation: weak correlation  $U = 1$ , intermediate correlation  $U = 2$ , and strong correlation  $U = 3$ .

For rather small disorder ( $W < 3$ ), at half-filling the three cases analyzed in Fig. 1 are different:<sup>22</sup> for  $U = 1$  the system is in a metallic phase, for  $U = 3$  it is in a Mott insulating phase (represented by the orange line at  $\delta = 0$  in the phase diagram), and  $U = 2$  is an intermediate case, since it is a Mott insulator for small disorder (orange line in Fig. 1) and a metal for intermediate  $W$ . It is well known that in the correlated case, upon doping the Mott insulator, states appear at the Fermi level.<sup>14</sup> Thus, for all the three values of  $U$  in Fig. 1 we observe a correlated metallic phase for a large range of doping and small disorder.

As disorder increases, a transition to AMI is seen in the three cases at a critical disorder  $W_c$ . For  $U = 1$  and  $U = 3$  at *small to intermediate values of doping*,  $W_c$  is practically doping independent, its value being smaller for  $U = 3$  than for  $U = 1$ . For the former,  $W_c$  is smaller than  $U$ , which is the critical disorder value separating

the correlated Mott insulator from the AMI at half-filling (end of the orange line in the phase diagram). If we now look at the results for  $U = 2$ , the (red)  $W_c$  line shows a dependence with doping: it is close to the half-filling value at small doping and, by increasing  $\delta$ , it decreases towards the same value observed for  $U = 3$  (compare  $W_c$  for  $U = 2$  and  $U = 3$  at  $\delta \approx 0.7$ ).  $W_c$  vs.  $\delta$  for  $U = 2$  thus interpolates between what is observed for  $U = 1$  and  $U = 3$ .

The comparison between the weak ( $U = 1$ ) and strong ( $U = 3$ ) correlated phase diagrams described above seems then to suggest that the metal that appears upon doping the Mott insulator is more susceptible to disorder induced localization than the metal which sets at small  $U$ . Indeed, if we compare the typical DOS for the different values of  $U$  at  $W = 1.5$ , shown in Fig. 2, we observe that  $\rho_{typ}(\omega)$  decreases as  $U$  increases. The transition occurs when  $\rho_{typ}(\omega)$  vanishes, since this indicates that extended states of the system fully localize (we will discuss this in more detail in Sec. IV A). This implies that the system with  $U = 3$  is closer to Anderson MIT than the one with  $U = 1$ . As a consequence of  $W_c$  being smaller for  $U = 3$  than for  $U = 1$ , the properties of the metal-AMI transition in the weak correlation (where V-shaped AMI arises, see next subsection for details) and the transition in the strong correlation regime (where a different AMI arises) are different. For even larger  $U$ , the properties of the system are similar to the ones at  $U = 3$  when we consider the same doping and disorder values (see Appendix A for details).

Moving now to large doping, for each  $U$  value it appears a region that we identify as a *band* AMI. In this case, while electronic states are always present at the Fermi level ( $\rho_{av}(\omega = 0) \neq 0$ ), the typical DOS that describes the extended states shifts to negative frequency and acquires a zero value at the Fermi level,  $\rho_{typ}(\omega = 0) = 0$ , like the DOS of a band insulator typically does (see section IV A for further details).

By further increasing disorder  $W$ , at small doping, the

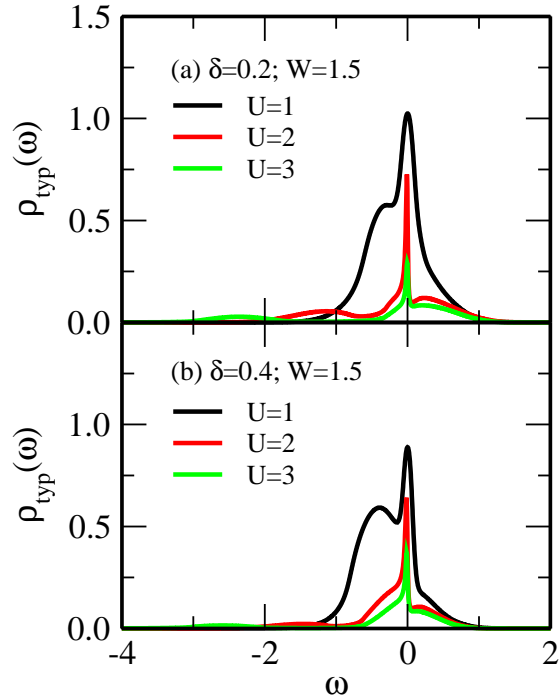


FIG. 2. Comparison of the typical DOS as a function of energy for  $U = 1$ ,  $U = 2$ , and  $U = 3$  at a disorder value chosen such that the systems are in the metallic phase. Although disorder is  $W = 1.5$  in all cases, as  $U$  increases the system is closer to the MIT.

AMI acquires a V-shaped DOS ( $\rho_{av}$ ) at the Fermi level. This V-shaped DOS AMI appears at all values of the interaction  $U$ , at an Anderson-Mott-like MIT in the small correlation regime ( $U = 1$ ) and as a crossover within the AMI phase in the strong correlation regime ( $U = 3$ ). We discuss the properties of this phase in detail in the following subsection.

### A. V-shaped DOS Anderson-Mott Insulator

We explore in this subsection how the V-shaped DOS arises within the AMI phase, in the large disorder region of the  $U = 3$  phase diagram of Fig. 1. This phase is the same kind of AMI that arises at the Anderson-Mott localization at half-filling (see the results for  $W = 3.5$  in Appendix B), as we shall show by displaying the spectral function.

In Fig. 3(a) we show  $\rho_{av}(\omega)$  as a function of frequency for  $\delta = 0.2$  and  $W = 4$ . (Results for other values of  $\delta$  are presented in Appendix C.) A zoom of the low energy region is presented in panel (b); a V-shaped DOS is clearly seen around the Fermi level. A V-shaped DOS has been observed also within other treatments of disorder. This is the case of the QMC simulations previously mentioned.<sup>25</sup> A suppression of the DOS is also obtained when solving the AHM at the Hartree-Fock level. In this case,

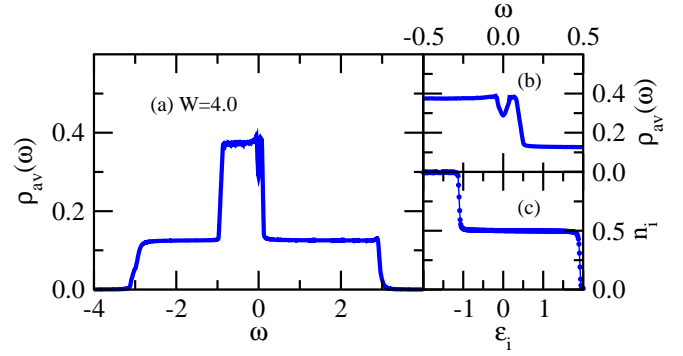


FIG. 3. (a) Average DOS  $\rho_{av}(\omega)$  as a function of energy for  $W = 4$  and  $\delta = 0.2$ , that is, for parameters inside the V-shaped AMI region of the phase diagram. (b) Zoom of the plot in panel (a) for energies around the Fermi level. (c) Occupation number per site and per spin as a function of the on-site energy for the system considered in panel (a). Other parameters used were  $U = 3$  and  $T = 0.01$ .

it has been observed in the insulating phase of one and three dimensional systems irrespective of the doping,<sup>31</sup> as well as in the metallic phase observed at half-filling in two dimensions.<sup>32</sup> Within these results, the size of the V shape is more pronounced than in our results. Though smaller, the V-shaped DOS is clearly present in the regions indicated in our phase diagram. We think that the smaller size of the V-shaped DOS in our calculations may be a consequence of the TMT approximation in the AMI phase, which corresponds to the atomic limit. This means the average DOS follows the bare distribution of  $\varepsilon_i$  and it is simply given, around  $\omega = 0$  and for  $W > U$ , by the superposition of two rectangles. The V-shaped DOS is thus located on “top” of these rectangles.

We now show that the V-shaped DOS phase is related to the appearance of empty sites. The occupation per site and per spin as a function of on-site energy corresponding to the DOS in Fig. 3(a) is shown in panel (c). Note that we have empty sites, besides those which are doubly- and singly-occupied. We have analyzed other values of  $\delta$  for  $U = 3$ , and the phase diagrams for  $U = 1$  and  $U = 2$  presented in Fig. 1, and concluded that the V-shaped AMI region always arises when empty sites appear in the system. We can understand better the role played by the empty sites in the formation of the V-shaped DOS by looking at the DOS for different single-impurity problems, as presented in detail in Appendix D.

We shall now analyze how the formation of the V-shaped AMI depends on doping  $\delta$  and interaction  $U$ . As doping increases, carriers are added to the system and more sites become doubly-occupied in comparison with a smaller  $\delta$ , as can be seen in Fig. 4(a). As a consequence, more disorder has to be added to the system [compare the results for  $W = 4.0$  and  $W = 4.75$  of the same figure for  $\delta = 0.3$ ] to empty some sites. The V-shaped DOS thus appears for larger values of disorder when the doping  $\delta$  increases, as we observe in the phase diagrams of

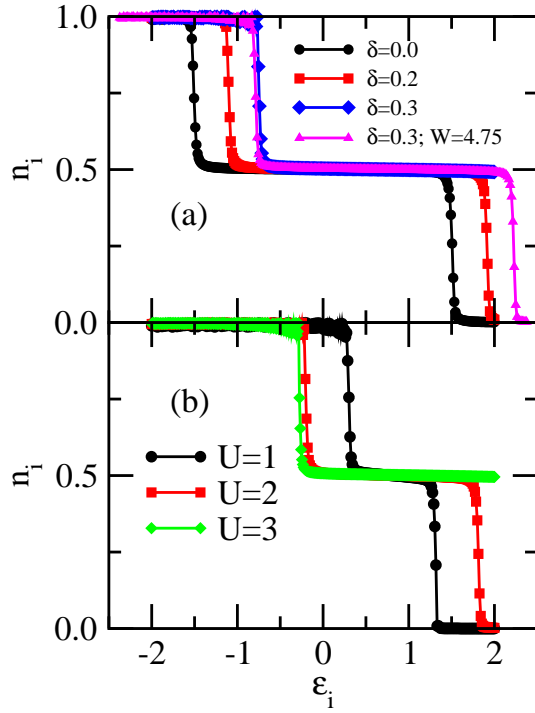


FIG. 4. (a) Site occupation per spin as a function of the on-site energy for different values of doping and  $W = 4$ , except for the magenta curve with triangles, for which  $W = 4.75$ . Other parameters used were  $U = 3$  and  $T = 0.01$ . (b) Site occupation per spin as a function of the on-site energy for different values of the electronic correlation. Other parameters used were  $W = 4$ ,  $\delta = 0.4$ , and  $T = 0.01$ .

Fig. 1.

We now show in Fig. 4(b) the occupation per site and per spin for  $W = 4$ ,  $\delta = 0.4$ , and the different values of  $U$ . Since single occupation is a characteristic of Mott insulators, the plateau at  $n_i = 0.5$  becomes larger as  $U$  increases. For the values of  $W$  and  $\delta$  considered in the figure, the empty sites present for  $U = 1$  and  $U = 2$  become occupied as we move to  $U = 3$ . Thus, empty sites “disappear” with either the increase of doping or correlations and, for large  $U$ , most of the disorder versus doping phase diagram corresponds to an AMI without a V-shaped DOS, as we describe in detail in the following section.

#### IV. RESULTS FOR $U = 3.0$

We shall now study the AMI without V-shaped DOS that appears by increasing interaction  $U$ , sandwiched between the V-shaped DOS AMI and the metal phases on a large part of the phase diagram. As we have mentioned above, the properties of this AMI phase are bound to the disappearance of empty sites. To this purpose, we con-

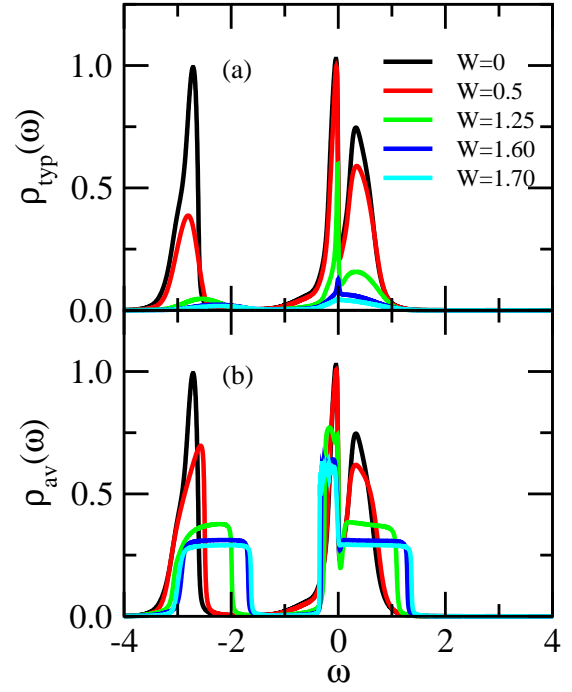


FIG. 5. (a) Typical and (b) average DOS as a function of energy for different values of disorder  $W$  and fixed doping  $\delta = 0.2$ . Other parameters used were  $U = 3$  and  $T = 0.01$ .

sider the  $U = 3$  case (Fig. 1c), and study the Anderson-Mott transition from the disordered metal by increasing the disorder strength  $W$  and various dopings  $\delta$ . We analyze in particular the behavior of typical and average DOS.

##### A. Metal-insulator transitions

The DMFT-TMT results for  $\rho_{typ}(\omega)$  and  $\rho_{av}(\omega)$  are shown, respectively, in panels (a) and (b) of Fig. 5 for fixed  $\delta = 0.2$  and different values of disorder  $W$ . Since we have small doping, the typical DOS presents a structure of three peaks: two Hubbard bands at high energies of the order of  $\pm U$  and a quasiparticle-like peak at the Fermi level  $\omega = 0$ , as it has been previously reported in the clean case.<sup>28</sup> According to our results, this holds for small disorder as well, characterizing the system as a metal in this region of parameters.

As disorder  $W$  increases, Anderson localization starts to play a role: its effects can be seen by comparing the results for  $\rho_{typ}(\omega)$  [panel (a)] and  $\rho_{av}(\omega)$  [panel (b)], since the former takes into account only extended states, while the latter includes both extended and localized states of the system. As  $W$  increases, states at the band edges localize<sup>15</sup> and we observe that the bands in the typical DOS become smaller. For even more disordered systems,  $\rho_{typ}(\omega)$  vanishes, signaling that the system has gone through a disorder-driven MIT. We notice that disorder acts differently on different energy scales. In  $\rho_{typ}(\omega)$

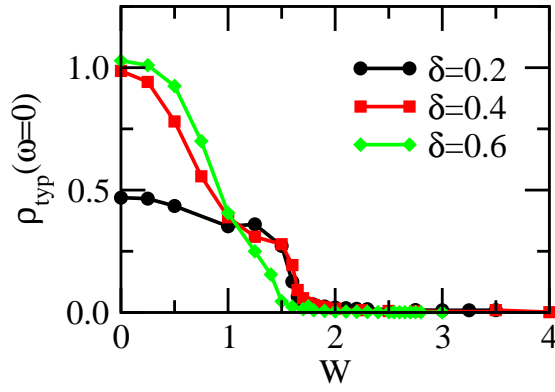


FIG. 6. Typical DOS at the Fermi level as a function of disorder for different values of doping. Results for  $\delta = 0.2$  correspond to  $\rho_{typ}(\omega)$  shown in panel (a) of Fig. 5. Other parameters used were  $U = 3$  and  $T = 0.01$ .

Hubbard-like bands around larger values of energy shrink faster than the quasiparticle-like one close to the Fermi level. Notice that  $\rho_{av}(\omega)$  remains instead finite at the Mott-Anderson transition. The general effect of disorder appears to be a spreading in energy of the spectral weight, both in the Hubbard bands and at the low-energy quasi-particle peak.

To determine the critical disorder  $W_c$  at which the MIT takes place, it is easier to track the typical DOS at the Fermi level as a function of disorder, as we display in Fig. 6 for different values of doping. This quantity plays the role of an order parameter for the disorder induced MIT, since it is different from zero in the metallic region ( $W < W_c$ ) and is zero in the Mott-Anderson insulator ( $W > W_c$ ). Based on the behavior of  $\rho_{typ}(\omega = 0)$  as a function of disorder, we have determined the transition line between the metallic and AMI phases shown in Fig. 1 (red filled dot line). Notice that for  $\delta = 0.2$  the maximum of  $\rho_{typ}(\omega)$  is close to  $\omega = 0$ , but not exactly at  $\omega = 0$  (in accordance with the results of Ref. 28); this explains why  $\rho_{typ}(\omega = 0) \approx 0.5$  for the clean system in Fig. 6, instead of the maximum value of  $\approx 1$  for  $\rho_{typ}(\omega)$  seen in Fig. 5(a).

A key observation is that there exists only a small dependence of  $W_c$  with doping  $\delta$ . As mentioned above and observed in Fig. 5(a), the transition to the AMI takes place when all extended states of the system localize. For fixed  $U = 3$  (see now Fig. 2), the range in energy where  $\rho_{typ}(\omega)$  extends is roughly doping independent. If doping increases, we observe mainly a transfer of spectral weight from above the Fermi level to energies below it. This might justify the fact that  $W_c$  is practically constant for small to moderate  $\delta$ . A similar behavior is observed for  $U = 1$ , but not in the intermediate case of  $U = 2$ , as we have discussed in Sec. III.

More interesting is the fact that  $W_c$  for the doped case is smaller than  $U$ , which is the critical disorder at which the transition from the Mott insulator to AMI is seen at half-filling (end of orange line in Fig. 1). This means that the doped Mott insulator is more susceptible to disorder

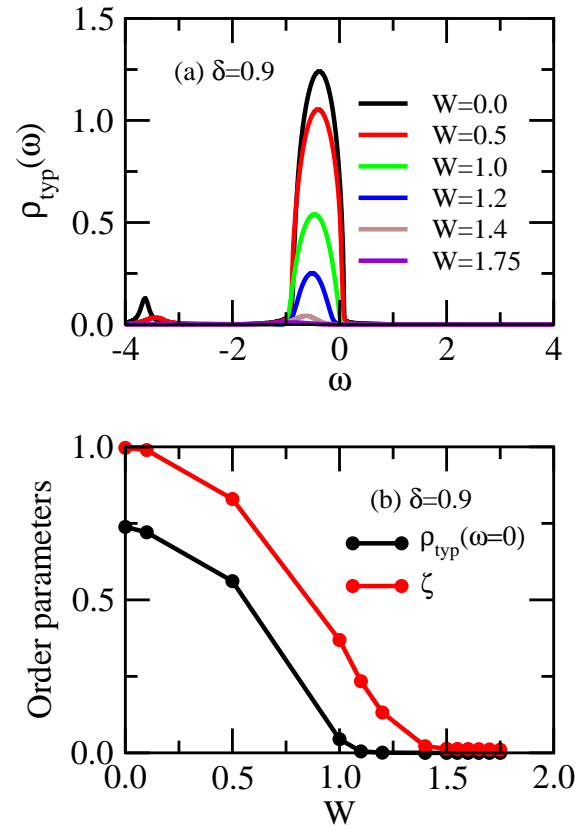


FIG. 7. (a) Typical DOS as a function of energy for different values of disorder  $W$  and fixed doping  $\delta = 0.9$ . (b) Typical DOS at the Fermi level and  $\zeta = \int_{-\infty}^{\infty} \rho_{typ}(\omega) d\omega$  as a function of disorder corresponding to the results in (a). Other parameters used were  $U = 3$  and  $T = 0.01$ .

induced localization, as we have already mentioned in Sec. III. By introducing carriers into the system in fact, a narrow band rises within the gap, as seen in our results in Fig. 5(a). By adding disorder to the doped system, this narrow band localizes at a disorder strength which is smaller than the one required to Anderson localize the Mott insulator, which requires that the wide Mott gap is filled due to disorder effects. (For details on how the transition is approached at half-filling see Appendix B.) As mentioned in the previous section, this is not observed for  $U = 1$  and  $U = 2$ , probably because for these values of  $U$  the system is in a metallic state at half-filling, and the wide Mott gap is replaced by a wide band of itinerant states around the Fermi level, that can Anderson localize only at higher disorder strengths.

For large doping ( $0.75 < \delta < 1.0$ ), we observe a region within AMI that, with abuse of language, we identify as a band AMI. Starting with the clean system,  $\rho_{typ}(\omega)$  shrinks as disorder increases, similar to what happens for small doping. However, for large doping,  $\rho_{typ}(\omega = 0)$  becomes zero for a smaller value of disorder ( $W_c$ ) than that at which the whole band vanishes ( $W_{c2}$ ). This means that for  $W_c < W < W_{c2}$  the system has still a band



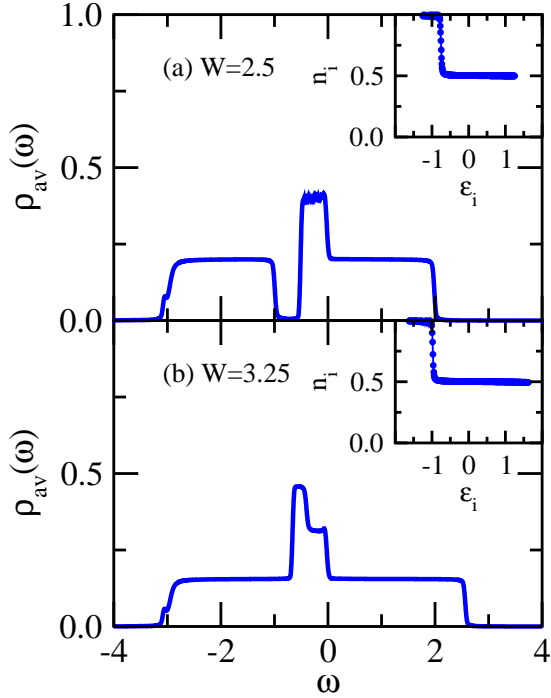


FIG. 8. Average DOS as a function of energy for  $U = 3$  and (a)  $W = 2.50$  and (b)  $W = 3.25$ . The insets show the occupation number per site and per spin as a function of the on-site energy for the same parameters of the results in the main panels. The doping in both cases is  $\delta = 0.2$ ; the temperature is  $T = 0.01$ .

of extended states, which is located below the Fermi energy. This behavior is exemplified in Fig. 7 for the case of  $\delta = 0.9$ : panel (a) shows  $\rho_{typ}(\omega)$  for different values of disorder, while panel (b) presents both  $\rho_{typ}(\omega = 0)$  and  $\zeta = \int_{-\infty}^{\infty} \rho_{typ}(\omega) d\omega$  as a function of  $W$ . As we can see, for this value of doping, the system enters into the insulating phase [ $\rho_{typ}(\omega = 0) = 0$ ] at  $W_c \approx 1.1$ , while all states are localized ( $\zeta = 0$ ) only at  $W_{c2} \approx 1.75$ . This behavior of  $\rho_{typ}(\omega = 0)$  at  $W_c$  is reminiscent of that of a band insulator, though the total spectral intensity  $\rho_{av}(\omega = 0)$  remains in all cases finite at the Fermi level. Note that  $W_{c2}$  approximately coincides with the disorder at which the system enters the AMI phase for  $\delta < 0.6$ , as expected if the vanishing of  $\zeta$  mainly depends on the  $U$  value.

### B. Character of the Anderson-Mott insulator

We want now to characterize the physical properties of the AMI phase. To this purpose, we shall focus on the (arithmetic) average DOS  $\rho_{av}(\omega)$  [defined in eq. (5)], which can be directly connected to spectroscopic experiments. Fig. 8 shows two examples of  $\rho_{av}(\omega)$  for  $\delta = 0.2$  and  $U = 3$ : one for which the disorder  $W < U$  [panel (a)] and another for which  $W > U$  [panel (b)]. In both cases the system is in the AMI phase, where all states are localized. Since the typical DOS is zero, meaning that

there is no bath for the impurities to hybridize, within our TMT approximation impurity sites are effectively in the atomic limit. In this case, in the absence of disorder  $\varepsilon_i$  the DOS of a single-impurity problem presents two Dirac delta peaks, one at  $\omega = -U/2$  and another at  $\omega = U/2$ . As disorder  $\varepsilon_i$  is added, these peaks spread in energy following the flat uniform distribution of the disorder. If disorder is large enough, these rectangles overlap at small frequencies, giving rise to the form of the average DOS seen in Fig. 8.

By looking at the results in panel (a), for  $W < U$ , we observe that there is a well defined gap at negative energies in  $\rho_{av}(\omega)$ . This profile for the DOS reminds us that of the slightly doped Mott insulator. In the case of  $W > U$  [panel (b)], on the contrary, a gap is not seen in  $\rho_{av}(\omega)$ . This reminds us of an Anderson insulator. In the insets of the panels, we show the corresponding occupation  $n$  per site and per spin as a function of the on-site energy  $\varepsilon$ . In both cases,<sup>24</sup> there are sites that are doubly occupied ( $n = 1$ ), as in an Anderson insulator, and sites that are singly-occupied ( $n = 0.5$ ), as in a Mott insulator (but no empty site as in the V-shaped AMI region). Since the two systems have characteristics of Anderson and Mott insulators, we identify both cases as AMI in the phase diagram of Fig. 1. However, we are tempted to say that in the case of panel (a) the role played by Mott mechanism of localization is stronger than that of Anderson effects. Indeed, the correlation  $U$  is larger than disorder  $W$  and a gap is observed in the average DOS. On the other hand, Anderson mechanism may dominate over the Mott one in the case where disorder is larger than correlations [panel (b)]. In the phase diagram, the first case is observed whenever  $W_c < W < U = 3$ , while the second corresponds to  $W > U = 3$ . Similar behavior occurs for  $U = 2$  and  $\delta > 0.5$ , for which there is a region where  $W_c < U$ .

We recall that at half-filling ( $\delta = 0$ ) the Mott dominated region for  $W < W_c \approx U$  presents only singly  $n = 0.5$  occupied sites, being double occupation  $n = 1$  absent.<sup>20</sup> On the other hand, for  $W > U$ , there exist doubly- and singly- occupied sites, as well as empty ones, and the average DOS has no gap. The presence of this third kind of sites - the empty ones - gives rise to the V-shaped DOS, as we described in the previous section.

### C. Crossover to the V-shaped DOS AMI

Finally, it is useful to see the behavior of the disorder as a function of chemical potential  $\mu$  for fixed doping, showed in Fig. 9. In the metallic phase (for small values of  $W$ ), the  $W$  vs.  $\mu$  curve is sharply vertical. By entering into the AMI, above  $W \approx 1.75$ , the  $W$  vs.  $\mu$  follows closely a linear law  $\mu = (\delta - 0.5)W + U$ . By further increasing disorder,  $W$  vs.  $\mu$  displays a sharp change in slope when entering into the V-shaped DOS AMI. For  $\delta$  values where V-shaped DOS is observed,  $\mu$  always increases with  $W$ .

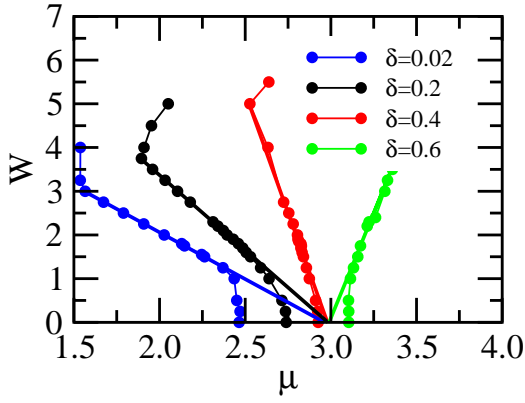


FIG. 9. Chemical potential  $\mu$  ( $x$ -axis) obtained to keep the values of  $\delta$  fixed considering different disorder strengths ( $y$ -axis). Straight lines correspond to fittings of the numerical results in the range where a linear behavior is observed; note that the lines meet at the point  $\mu = U = 3$ . Other parameters used were  $U = 3$  and  $T = 0.01$ .

The linear  $W$  vs.  $\mu$  behavior in the AMI region allows us to establish an equation determining the disorder dependence of the line separating the V-shaped and not V-shaped DOS AMI. We profit that within our method in the AMI each impurity site is in the atomic limit (see Appendix D). In this case, the site is empty if its on-site energy  $\varepsilon_d = \varepsilon_i - \mu > 0$ . The value of the disorder where the first empty site forms must coincide with the highest possible value of on-site energy  $\varepsilon_i = W/2$ , i.e.  $W/2 = \mu$ . Plugging this value of  $\mu$  into the  $W$  vs.  $\mu$  linear relation, which holds up to the transition into the V-shaped DOS region, we obtain:

$$W = \frac{U}{1 - \delta}. \quad (6)$$

Equation 6, which we display in Fig. 1 as a dashed gray line, well describes the V-shaped DOS crossover within the AMI phase that we establish numerically (brown diamond symbols in the figure). This confirms the relationship between V-shaped DOS AMI and the appearance of empty sites within the insulator phase.

## V. CONCLUSION

In this work, we have solved the Anderson-Hubbard model in the doped case by using the combination of Dynamical Mean Field Theory and Typical Medium Theory. The former describes the Mott transition, while the latter takes into account Anderson localization effects. We have built the disorder versus doping phase diagram for three values of  $U$ :  $U = 1$ ,  $U = 2$ , and  $U = 3$ , in units of the clean, non-interacting bandwidth. For any interaction we observe an Anderson-Mott insulating phase similar to the one that exists at half-filling. It presents a V-shaped

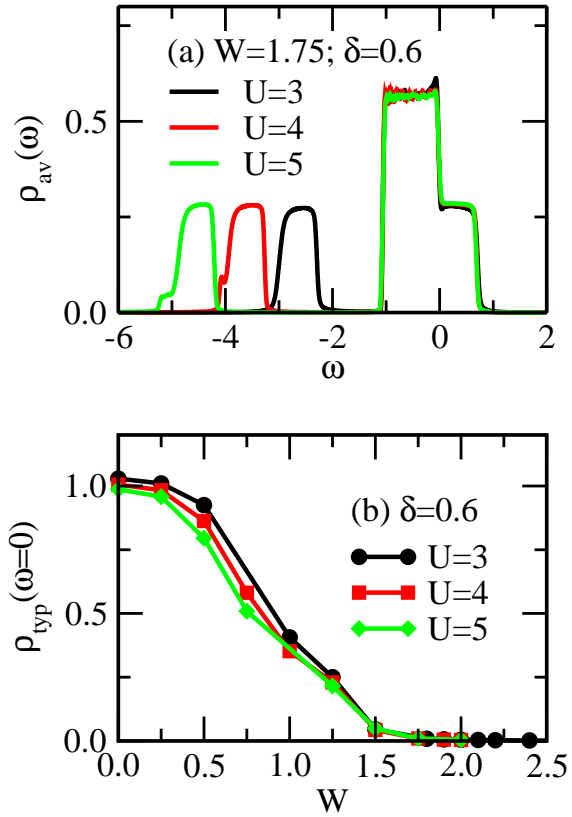


FIG. 10. Results for large values of the interaction,  $U = 3$ ,  $U = 4$ , and  $U = 5$ . (a) Average DOS when  $W = 1.75$ . (b) Typical DOS at the Fermi level as a function of  $W$ , showing that the order parameter goes to zero for the same value of  $W_c$  (for  $U \geq 3$ ). Other parameters used were  $\delta = 0.6$  and  $T = 0.01$ .

DOS around the Fermi level, which we show to be related to the presence of empty sites in the system. As doping (and thus the number of carriers in the system) increases, the empty sites that exist at small doping become occupied; as a consequence, the V-shaped DOS is no more observed. In addition, when the electronic interaction becomes stronger, the region without a V-shaped DOS increases. For  $U = 3$ , a large part of the disorder versus doping phase diagram corresponds to an Anderson-Mott insulator without the presence of a V-shaped DOS close to the Fermi level. When there is a large number of electrons, the system is strongly influenced by the combined effect of disorder, interaction, and doping to form an insulator.

## ACKNOWLEDGMENTS

We acknowledge Eduardo Miranda for discussions and Jaksa Vučičević and Darko Tanasković for the development of the IPT single-impurity code used in our calculations. This work is supported by FAPEMIG, CNPq (in particular through INCT-IQ



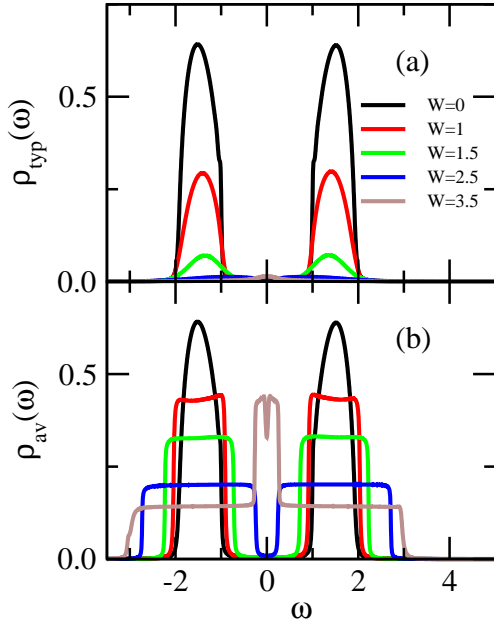


FIG. 11. (a) Typical and (b) average DOS as a function of energy for different values of disorder  $W$  at half-filling. Other parameters used were  $U = 3$  and  $T = 0.01$ .

465469/2014-0), and CAPES (in particular through programs CAPES-COFECUB-0899/2018 and CAPES-PrInt-UFGM (M.C.O.A.)).

#### Appendix A: Spectra and metal-insulator transition at strong $U > 3$

We shall show here that the results on the MIT that we established for the  $U = 3$  case are qualitatively similar for larger interaction  $U$ . Interaction has the effect of changing the position of the DOS bands. In the presence of doping, only the low energy band moves proportionally to the  $U$  value. A quasiparticle-like band remains around the Fermi level; its position does not change by increasing  $U$  to keep the doping  $\delta$  fixed. In Fig. 10(a), where we display the average DOS  $\rho_{av}(\omega)$ , we can see an example of this behavior: increasing the interaction does not change the Fermi level band. This causes the value of  $W_c$  not to change, as can be seen in Fig. 10(b). This phenomenon only occurs when the bands are far apart (in the Mott regime  $W < U$  of the doped AHM).

#### Appendix B: Results for $U = 3$ at half-filling

The evolution of the typical and average DOS as disorder increases for the case of  $U = 3$  and no doping is presented in Fig. 11. The clean system has a Mott gap, which starts to be filled with localized states as disorder increases. The gap eventually closes at the critical disorder at which the MIT takes place. This behavior is

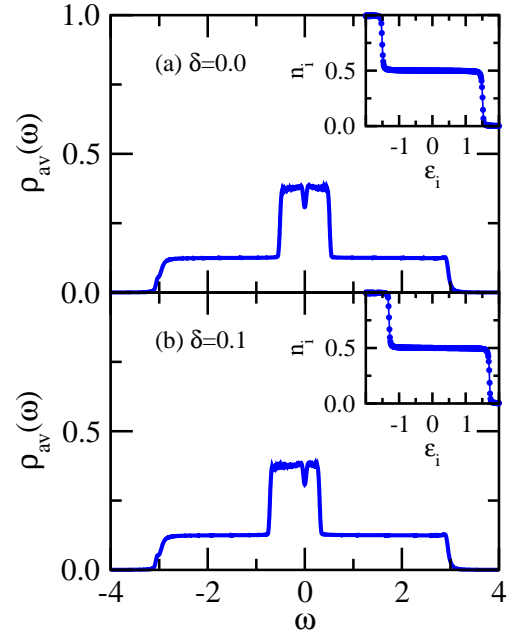


FIG. 12. Average DOS  $\rho_{av}(\omega)$  as a function of energy for (a)  $\delta = 0$  and (b)  $\delta = 0.1$ , which can be compared to the results for  $\delta = 0.2$  in Fig. 3. Insets show the occupation per site and per spin as a function of  $\varepsilon$  corresponding to the results in the main panels. Other parameters used were  $W = 4$ ,  $U = 3$ , and  $T = 0.01$ .

different than the one presented in Fig. 5 for the doped case, where the clean system is a metal. The V-shaped DOS is observed at half-filling for all  $W > W_c$ , as illustrated in the figure for  $W = 3.25$ .

#### Appendix C: V-shaped DOS for different $\delta$

When the V-shaped DOS exists, it is interesting to look at its evolution as the doping changes, for fixed value of disorder. The V-shaped DOS is always observed close to  $\omega = 0$ , but it changes position relatively to its “background”. This can be seen when comparing the results in Fig. 3 for  $\delta = 0.2$  with those at half-filling ( $\delta = 0$ ) and for  $\delta = 0.1$ , which are in Fig. 12. While in the symmetric case the V is in the middle of the “top rectangle”, as it might be, it moves to the right edge as  $\delta$  increases. Note that the V-shaped DOS is present at half-filling in the entire AMI phase. This is because in this case  $W_c \approx U$  and, according to the two-fluid picture of the AMI,<sup>24</sup> empty sites exist in the system for every  $W > U$ .

#### Appendix D: Formation of V-shaped DOS

As mentioned in the main text, we can understand better the role played by the empty sites in the formation of the V-shaped DOS by looking at the DOS for different single-impurity problems. In Fig. 13 we present it as a

function of energy for a *few* chosen on-site energies. Note that  $\rho_{av}(\omega)$  shown in Fig. 3(a) is calculated by performing an average over 300 of these single-impurity problems, with  $\varepsilon$  ranging from  $-W/2$  to  $W/2$ .

In the DMFT-TMT description of the AMI, the bath that the impurities “see” vanishes, which means that effectively we are in the atomic limit of the single-impurity problems, as previously mentioned. In this case, the impurity ( $d$ -electron) Green’s function is given by<sup>33</sup>

$$G_{d\sigma}(\omega) = \frac{1 - \langle n_{d-\sigma} \rangle}{\omega - \varepsilon_d} + \frac{\langle n_{d-\sigma} \rangle}{\omega - \varepsilon_d - U}, \quad (D1)$$

where  $\varepsilon_d = \varepsilon - \mu$  is the impurity local energy [ $\varepsilon$  is the on-site energy in the original AHM - see eq. (1)]. For very small, negative values of  $\varepsilon$ , the two poles are below the Fermi level, implying that  $\langle n_{d-\sigma} \rangle = \langle n_{d\sigma} \rangle = 1$  and that, according to eq. (D1), the DOS presents only one peak. This peak moves to larger values of  $\omega$  when  $\varepsilon$

increases, as we can see in panels (a) and (b) of Fig. 13. Once  $\varepsilon$  increases towards zero, the single-impurity DOS has contributions from two peaks, one below and another above the Fermi level - see panels (c), (d), and (e). As we move to higher, positive values of  $\varepsilon$ , the two poles move above the Fermi level, which means that  $\langle n_{d-\sigma} \rangle$  and  $\langle n_{d\sigma} \rangle$  tends to vanish. In this case, the single-impurity DOS presents again only one peak, above the Fermi level, as exemplified in panels (f) and (g).

We can estimate the average DOS by looking at the maximum value  $h_{max}$  of the single-impurity DOS as a function of the energy  $\omega_{max}$  at which this maximum value occurs for different on-site energies, which we plot in panel (h) of Fig. 13. As we can see, around zero energy  $h_{max}$  first decreases and then increases, following the shape of  $V$ . This is exactly the behavior seen in the computed average DOS shown in Fig. 3(b). Note that the increase of  $h_{max}$  for positive, small values of energy happens due to the presence of the empty sites, represented by green symbols in panel (h).

- 
- <sup>1</sup> N. F. Mott, Metal-insulator transitions (Taylor and Francis, 1974).
  - <sup>2</sup> J. Hubbard, Proceedings of the Royal Society of London. Series A. Mathematical and Physical Sciences **281**, 401 (1964).
  - <sup>3</sup> M. Imada, A. Fujimori, and Y. Tokura, Rev. Mod. Phys. **70**, 1039 (1998).
  - <sup>4</sup> E. Dagotto, Science **309**, 257 (2005).
  - <sup>5</sup> D. McWhan, A. Menth, J. Remeika, W. F. Brinkman, and T. Rice, Phys. Rev. B **7**, 1920 (1973).
  - <sup>6</sup> P. Limelette, A. Georges, D. Jérôme, P. Wzietek, P. Metcalf, and J. Honig, Science **302**, 89 (2003).
  - <sup>7</sup> P. W. Anderson, Phys. Rev. **109**, 1492 (1958).
  - <sup>8</sup> P. A. Lee and T. Ramakrishnan, Rev. Mod. Phys. **57**, 287 (1985).
  - <sup>9</sup> E. Miranda and V. Dobrosavljević, Reports on Progress in Physics **68**, 2337 (2005).
  - <sup>10</sup> E. Abrahams, S. V. Kravchenko, and M. P. Sarachik, Rev. Mod. Phys. **73**, 251 (2001).
  - <sup>11</sup> S. V. Kravchenko and M. P. Sarachik, in 50 Years of Anderson Localization, edited by E. Abrahams (World Scientific, Singapore, 2010) Chap. 17, pp. 361–384.
  - <sup>12</sup> E. Lahoud, O. N. Meetei, K. B. Chaska, A. Kanigel, and N. Trivedi, Phys. Rev. Lett. **112**, 206402 (2014).
  - <sup>13</sup> Z. Wang, Y. Okada, J. O’Neal, W. Zhou, D. Walkup, C. Dhital, T. Hogan, P. Clancy, Y.-J. Kim, Y. Hu, et al., Proceedings of the National Academy of Sciences **115**, 11198 (2018).
  - <sup>14</sup> A. Georges, G. Kotliar, W. Krauth, and M. J. Rozenberg, Rev. Mod. Phys. **68**, 13 (1996).
  - <sup>15</sup> J. M. Ziman, Models of disorder (Cambridge University Press, 1979).
  - <sup>16</sup> V. Dobrosavljević, A. A. Pastor, and B. K. Nikolić, Europhys. Lett. **62**, 76 (2003).
  - <sup>17</sup> S. Mahmoudian, S. Tang, and V. Dobrosavljević, Phys. Rev. B **92**, 144202 (2015).
  - <sup>18</sup> A. Ostlin, Y. Zhang, H. Terletska, F. Beiușeanu, V. Popescu, K. Byczuk, L. Vitos, M. Jarrell, D. Vollhardt, and L. Chioncel, Phys. Rev. B **101**, 014210 (2020).
  - <sup>19</sup> K. Byczuk, W. Hofstetter, and D. Vollhardt, Phys. Rev. Lett. **94**, 056404 (2005).
  - <sup>20</sup> M. C. O. Aguiar, V. Dobrosavljević, E. Abrahams, and G. Kotliar, Phys. Rev. Lett. **102**, 156402 (2009).
  - <sup>21</sup> K. Byczuk, W. Hofstetter, and D. Vollhardt, Phys. Rev. Lett. **102**, 146403 (2009).
  - <sup>22</sup> H. Bragança, M. C. O. Aguiar, J. Vučičević, D. Tanasković, and V. Dobrosavljević, Phys. Rev. B **92**, 125143 (2015).
  - <sup>23</sup> J. Skolimowski, D. Vollhardt, and K. Byczuk, Phys. Rev. B **92**, 094202 (2015).
  - <sup>24</sup> M. C. O. Aguiar, V. Dobrosavljević, E. Abrahams, and G. Kotliar, Phys. Rev. B **73**, 115117 (2006).
  - <sup>25</sup> S. Chiesa, P. B. Chakraborty, W. E. Pickett, and R. T. Scalettar, Phys. Rev. Lett. **101**, 086401 (2008).
  - <sup>26</sup> D. B. McWhan, T. M. Rice, and J. P. Remeika, Phys. Rev. Lett. **23**, 1384 (1969).
  - <sup>27</sup> D. B. McWhan, J. P. Remeika, T. M. Rice, W. F. Brinkman, J. P. Maita, and A. Menth, Phys. Rev. Lett. **27**, 941 (1971).
  - <sup>28</sup> H. Kajueter and G. Kotliar, Phys. Rev. Lett. **77**, 131 (1996).
  - <sup>29</sup> M. Potthoff, T. Wegner, and W. Nolting, Phys. Rev. B **55**, 16132 (1997).
  - <sup>30</sup> T. Wegner, M. Potthoff, and W. Nolting, Phys. Rev. B **57**, 6211 (1998).
  - <sup>31</sup> H. Shinaoka and M. Imada, Phys. Rev. Lett. **102**, 016404 (2009).
  - <sup>32</sup> J. C. Szabo, K. Lee, V. Madhavan, and N. Trivedi, Phys. Rev. Lett. **124**, 137402 (2020).
  - <sup>33</sup> A. Hewson, The Kondo Problem to Heavy Fermions (Cambridge University Press, 1997).

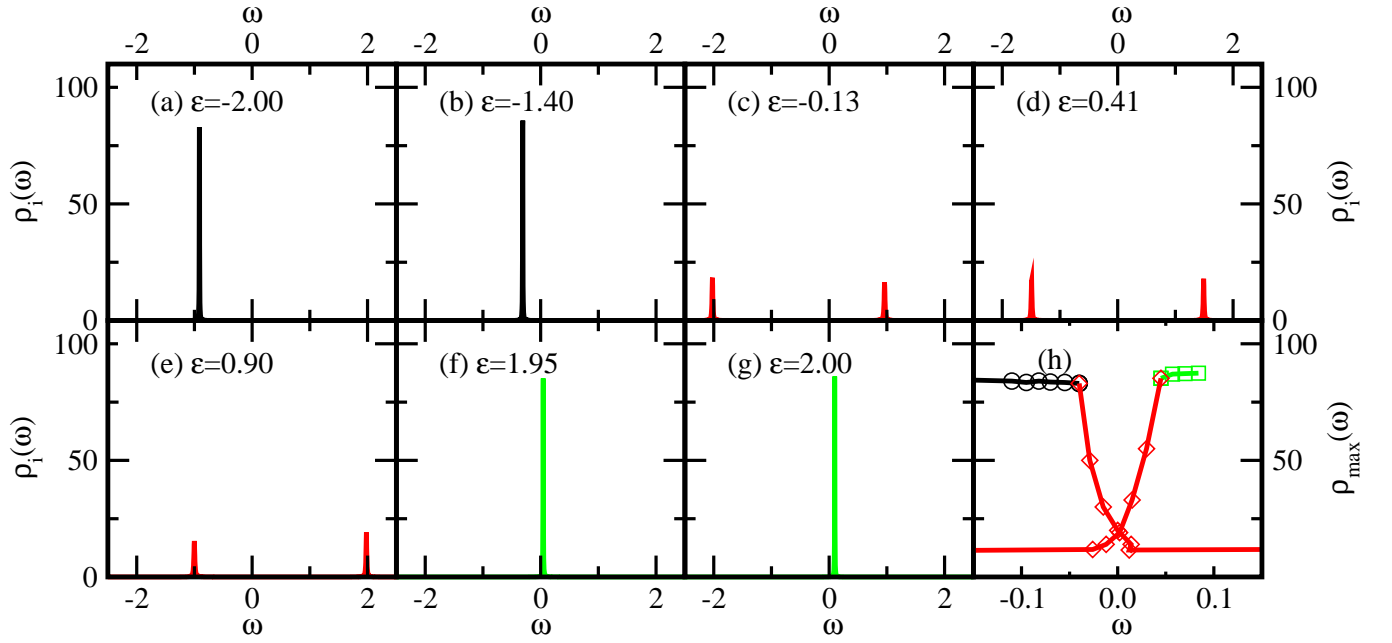


FIG. 13. (a)-(g) Single-impurity DOS as a function of energy for the different values of the on-site energy  $\varepsilon$  indicated in the panels. The impurity ( $d$ -electron) energy is  $\varepsilon_d = \varepsilon - \mu$ , where  $\mu \approx 1.91$  for the parameters considered in this figure. For  $\varepsilon$  values in (a) and (b), we have double occupation (which we indicate in black) and the DOS presents one peak at  $\varepsilon_d + U$ . In (c) to (e), the DOS presents one peak at  $\varepsilon_d$ , which corresponds to an occupied state, and another at  $\varepsilon_d + U$ , which is above the Fermi level and thus empty; this case is indicated in red. Finally, in (f) and (g) the states are empty, which we indicate in green, and the DOS shows one peak at  $\varepsilon_d$ . (h) Maximum value of the single-impurity DOS  $\rho_{\max}$  as a function of the energy  $\omega_{\max}$  at which this maximum value occurs for different values of  $\varepsilon$ , showing the formation of a V-shaped DOS around  $\omega = 0$ . Other parameters used were  $W = 4$ ,  $\delta = 0.2$ ,  $U = 3$ , and  $T = 0.01$ .